Original Direct Synthesis of Nanostructured MnO2 in Water by Hydroxylated Ammonium-Assisted Redox Process

Oriane Delaunay, Audrey Denicourt-Nowicki, Alain Roucoux

RESEARCH ARTICLE

Particle & Particle Systems Characterization
www.particle-journal.com

Original Direct Synthesis of Nanostructured MnO_2 in Water by Hydroxylated Ammonium-Assisted Redox Process

Oriane Delaunay, Audrey Denicourt-Nowicki, and Alain Roucoux**

Well-defined MnO_2 nanoworms are easily synthesized in water through an original redox process, using a cheap $KMnO_4$ precursor and a lipophilic hydroxylated quaternary ammonium. This phase-transfer agent can act as both a reducing and protective agent to avoid particles agglomeration. The concomitant formation of a zwitterionic betaine derivative is evidenced in this surfactant-assisted process. Interestingly, these nanomaterials demonstrate pertinent potentialities in cycloalkanes oxidation with a selectivity toward the corresponding ketones in neat water.

1. Introduction

In the drive toward eco-responsible chemistry, the use of earth-abundant and thus cheaper first-row transition metals (Mn, Fe, Co, Ni, or Cu), also called "biometals," has emerged as a novel promising trend in nanotechnologies.[1,2] Among them, manganese presents also an environmental compatibility, low toxicity, and a moderate cost[3] being the twelfth most abundant element in the Earth's crust with a concentration ≈950 g per ton.[4] Over the past decade, nanometer-sized manganese materials possessing different sizes and shapes, such as nanorods,[5] nanowires,[6] nanosheets,[7] nanoflakes[8,9] or koosh balls[10] have been synthesized using various synthetic approaches.[1,11] Among them, manganese dioxide designed as well-defined nanostructures, has known great interest as a relevant candidate for advanced applications in sensing,[12–14] energy storage[15–18] and also catalysis, such as the oxygen reduction reaction,[19,20] the remediation of pollutants,[21,22] or the oxidation of various substrates such as alcohols,[23–25] or alkylarenes.[26,27] The control of the morphology and the size of these nanoparticles remains essential to ensure a good reproducibility of the targeted performances specifically in terms of activity and selectivity in catalysis. However, the manganese dioxide tends to aggregate during the growth process, leading to larger and thus less active particles.[28] Thus, there is still a need to develop efficient and sustainable methodologies to synthesize well-defined MnO_2 nanoparticles.

Herein, starting from $KMnO_4$ in pure water, we present a direct and original one-pot redox process to design MnO_2 nanoworms under mild conditions (50 °C), using HEA16Cl (namely, N,N-dimethyl-N-cetyl-N-(2-hydroxyethyl) ammonium chloride), a cationic surfactant bearing a hydroxylated polar head (**Figure 1**) and without using an external reducing agent such as sodium borohydride. Finally, the potentialities of MnO_2 species were evaluated in the challenging Csp^3-H activation of cycloalkanes.[29]

2. Results and Discussion

In this strategy, the hydroxylated ammonium surfactant plays several essential roles in the particle growth process, acting as an electron donor to reduce the metallic precursor ($KMnO_4$), as well as a protective agent to efficiently maintain the Mn nanospecies within the aqueous phase. First, a 3 electrons mechanism for the reduction-oxidation (redox) process could involve the Mn^{7+} species from the salt precursor and the primary alcohol function of HEA16Cl, leading to MnO_2 particles simultaneously to the formation of a betaine derivative, namely N-carboxymethyl-N,N-dimethyl-1-hexadecanaminium (**Figure 2**). The formation of this cetylbetaine derivative was evidenced by several structural analyses on the MnO_2 colloidal suspension, such as Fourier transform infrared (FT-IR) and nuclear magnetic resonance (NMR) spectroscopies. The results were compared to those obtained on the two-step synthesis of the cetylbetaine according to a procedure adapted from the literature.[30]

Thus, the FT-IR spectrum of the prepared aqueous MnO_2 suspension shows an absorption peak ≈1633 cm^{-1}, characteristic of the zwitteronic carboxylate CO band. This peak is also found at 1627 cm^{-1} on the spectrum of the synthesized cetylbetaine derivative used as reference (**Figure 3**). Moreover, the ^1H NMR spectrum of the aqueous MnO_2 suspension reveals characteristic proton peaks of the cetylbetaine (Figure S1, Supporting Information), particularly the two protons of the methylene group at α the position of the carbonyl function ($\delta = 3.76$ ppm) and the two methyl groups linked to the quaternary nitrogen ($\delta = 3.17$ ppm). These values are in agreement with those observed for the as-synthesized cetylbetaine.

O. Delaunay, A. Denicourt-Nowicki, A. Roucoux
Univ Rennes, Ecole Nationale Supérieure de Chimie de Rennes, CNRS, ISCR – UMR6226
Rennes F-35000, France
E-mail: audrey.denicourt@ensc-rennes.fr; alain.roucoux@ensc-rennes.fr

The ORCID identification number(s) for the author(s) of this article can be found under https://doi.org/10.1002/ppsc.202400241

DOI: 10.1002/ppsc.202400241

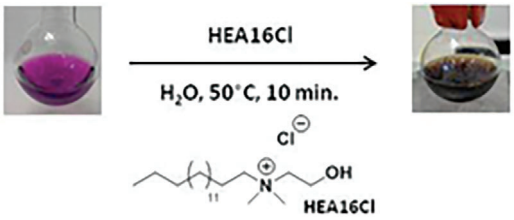

Figure 1. Original one-pot hydroxylated ammonium-assisted redox synthesis of MnO_2 nanoparticles.

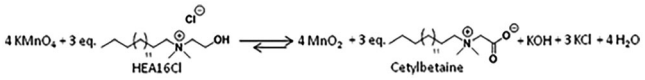

Figure 2. Proposed redox process for the MnO_2 nanoparticles formation.

Thus, it seems obvious that 3 equivalents (3 equiv.) of HEA16Cl are consumed to reduce the $KMnO_4$ precursor into MnO_2 particles, leading to the formation of cetylbetaine. Nevertheless, in these conditions (3 equiv. of HEA16Cl), the aqueous suspension of MnO_2 nanospecies tends to destabilize, giving rise to the formation of aggregates. An increase in the HEA16Cl to 5 equivalents leads to stable particles, thus proving the efficient role of the ammonium surfactant as a protective agent. Further complementary experiments showed that the betaine zwitterion formed during the redox process is not efficient in stabilizing the MnO_2 particles, thus contributing to their aggregation, in the presence of 3, 5, or even 10 equivalents (**Figure 4**, Pathway A). In addition, to mimic the formation of 3 equiv. of the zwitterionic derivative during the catalyst preparation, a suspension synthesized with HEA16Cl (2 equiv.) and the zwitterionic cetylbetaine (3 equiv.) was prepared at room temperature from $KMnO_4$ using $NaBH_4$ as a reducing agent (Figure 4, Pathway B). The aqueous solution of MnO_2 nanoparticles becomes dark brown and remains stable for several days due to the presence of the chlorinated surfactant acting as an efficient protective agent.

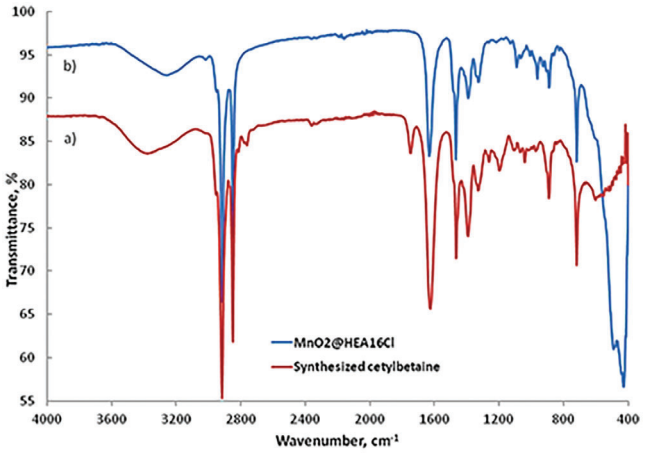

Figure 3. Comparison of the FT-IR spectra of the MnO_2@HEA16Cl suspension (in blue) and the as-synthesized cetylbetaine (in red).

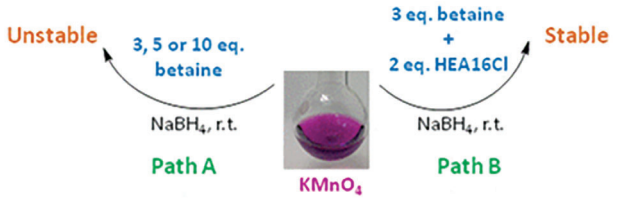

Figure 4. Studies on the catalyst stability according to the protective agent.

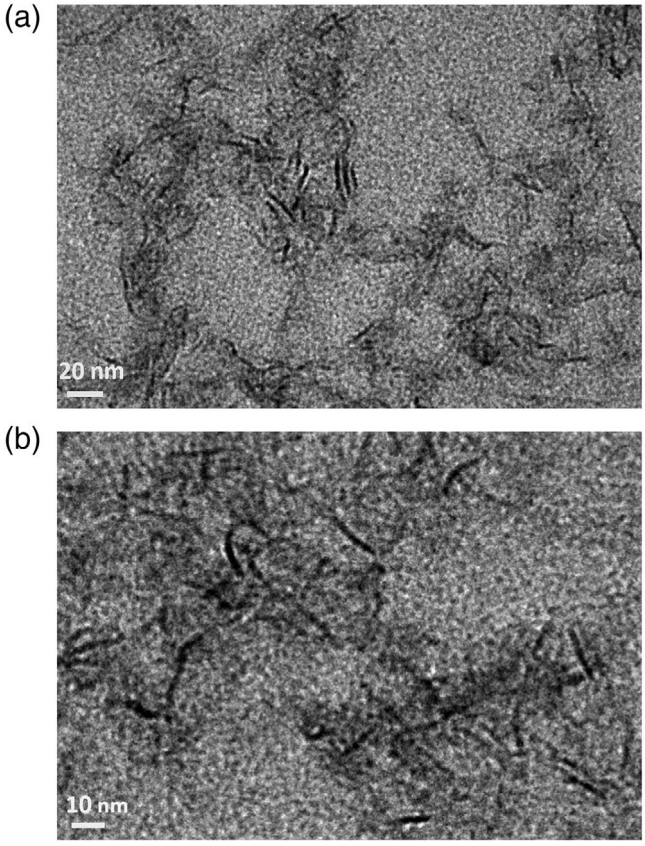

Figure 5. a) A representative TEM image of as-synthesized MnO_2 nanoworms (scale bar = 20 nm). b) A close-view TEM Image of the aqueous MnO_2@HEA16Cl suspension (scale bar = 10 nm).

Thus, the use of 5 equivalents of HEA16Cl is necessary, among which 3 equivalents being involved in the redox process of MnO_2 nanoparticles formation and the two others ensuring their stabilization and dispersion in the aqueous phase.

The Transmission Electron Microscopy (TEM) images of the as-synthesized aqueous MnO_2 suspension (**Figure 5**) show the formation of worm-shaped particles. The average length is 16 ± 1 nm, determined by measuring over 100 nanoworms, with a thickness of about 2 nm (Figure S2, Supporting Information). The aspect ratio, defined as the ratio of the length to the width, is centered ≈8. Such morphologies could be explained via a self-aggregation of various smaller particles, giving rise to nanoworm-like MnO_2 particles as already suggested in the literature.[31,32] This hydroxylated ammonium-assisted process is quite comparable to the morphology control on gold nanoparticles reported by J. Murphy's group.[33] From UV–vis absorption spectrum (Figure S3, Supporting Information), the as-synthesized MnO_2 nanoworms exhibited a broad absorption band centered ≈380 nm, which could be attributed to

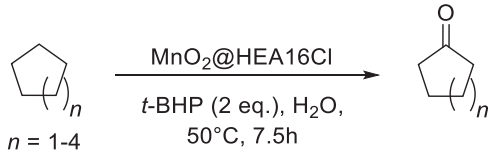

Figure 6. Cycloalkane oxidation reactions in water by *tert*-butylhydroperoxide under mild conditions.

the d–d transition of Mn ions, as already reported in the literature.[34] Moreover, the disappearance of the two main characteristic peaks of the Mn^{7+} ions, respectively located at 525 and 545 nm, proved the complete reduction of Mn(VII) to Mn(IV) species.[35,36]

Electron paramagnetic resonance (EPR) spectroscopy was applied to further validate the oxidation state of Mn species. A preliminary analysis was performed on a solid sample of the colloidal MnO_2 suspension obtained after lyophilization and compared to commercial MnO_2 powder as a reference (Figure S4, Supporting Information). EPR spectra parameters of the MnO_2@HEA16Cl colloidal suspension show a resonance signal at 3170 G with a g-factor of 2.13, which is characteristic of the hyperfine core-electron coupling of Mn^{4+} species, as also assigned in the literature for different α-MnO_2 nano shapes.[37] These values and the form of the line are identical to those observed for commercial MnO_2 used as a reference.

The potential catalytic activities of the nanosized MnO_2 system were estimated in the oxidation reaction of several cyclic hydrocarbons in reference to investigations of our group about ruthenium nanoparticles[38,39] (**Figure 6**).

This Csp^3-H functionalization remains of great interest for the industrial community,[28,40] affording key intermediates for the production of polyamides such as Nylons,[41] or for perfumery such as Jasmon.[42] The oxidation reaction was performed in the presence of *tert*-butylhydroperoxide as oxidant and in water as reaction media, at 50 °C.[43] The 70% w/w aqueous *t*-BHP solution was chosen as a suitable oxidant, owing to its higher safety and cost compared to the organic ones,[44] and also as an eco-responsible reagent, only producing *tert*-butanol as a by-product, which could be easily recycled.[45] The results are gathered in **Table 1**.

Under the reaction conditions involved, the conversion of the hydrocarbon increases according to the ring size, from 5% for cyclopentane to 36% for cyclooctane. Moreover, it is noteworthy to underline that in similar conditions, cyclooctane oxidation doesn't occur when using commercial MnO_2, even after calcination (3 h at 300 °C). This result could be explained by the poor water-solubility of the commercial MnO_2 as well as the absence of *t*-BHP consumed. In all cases, whatever the ring size is, a complete selectivity toward the corresponding cycloalkanone is achieved. In such processes, selectivity remains a crucial parameter to avoid the formation of undesirable over-oxidation co-products (mono- or di-carboxylic acids,...). For example, in the cyclohexane oxidation process, the industrial conversions are usually very low (≈5–6%), with a recycling of the substrate, to achieve high selectivity in KA oil to produce Nylon 6.6 via adipic acid as a key intermediate.[46] In this work, the complete selectivity toward cyclohexanone obtained with MnO_2 nanoparticles is particularly relevant for the production of Nylon 6 through ϵ-caprolactam.

Table 1. Catalytic performances of MnO_2 species in the oxidation reaction of various cycloalkanes.

Entry	Cycloalkane[a)]	Conversion[b)] [%]	Selectivity[b)] [%]
1	Cyclopentane	5	99
2	Cyclohexane	14	100
3	Cycloheptane	23	100
4	Cyclooctane	36	100

[a)] Reaction conditions: Cycloalkane (2.23 mmol, 1 equiv.), *t*-BHP (4.46 mmol, 2 equiv.), Substrate/Metal ratio = 117, 5 mL H_2O, 50 °C, 7.5 h; [b)] Determined by gas chromatography analyses using chlorobenzene as an internal standard.

3. Conclusion

In summary, well-controlled MnO_2 nanoworms were synthesized by an easy straightforward, and green redox process of $KMnO_4$ in the presence of a hydroxylated quaternary ammonium (HEA16Cl), double-acting as a reducing and protective agent. Extensive studies on the reduction mechanism of Mn^{7+} into Mn^{4+} have shown the formation of a zwitterionic cetylbetaine compound, thus confirming the oxidation of the hydroxyl function of the surfactant during the reduction process. Moreover, the role of HEA16Cl as a stabilizing agent was validated upon stability experiments on the colloidal suspension. Interestingly, preliminary catalytic oxidation reactions on various cycloalkanes allowed for achieving promising conversion up to 36%, with a complete selectivity toward the corresponding ketone. Considering its encouraging catalytic performances and low cost, MnO_2 nanorods could constitute a relevant catalytic alternative to noble metal nanoparticles for future eco-responsible oxidation processes and new perspectives in nanocatalysis.

4. Experimental Section

Chemicals: Chemical reagents, as well as potassium permanganate ($KMnO_4$) were purchased from Sigma–Aldrich, Acros Organics, and used without further purification. The *t*-BHP solution (Luperox TBH70X, 70% wt. in H_2O) was supplied by Acros Organics. Water was distilled twice before use by conventional methods.

Characterization: 1H and 13C NMR spectra were recorded on a Brucker Avance III 400 spectrometer at room temperature operating at 400.13 MHz for 1H and 100.61 MHz for 13C. The solvents used were chloroform, methanol, DMSO, or deuterium oxide. Chemical shifts were given as δ in part per million (ppm) with the peak of solvent used as a reference.

LC-MS spectra were recorded using the Shimadzu LCMS-2020 in ENSCR (Prominence UFLC coupled with single quadrupole mass spectrometer at ultra-high speed) with ionization by electrospray injection in positive mode (SM-ESI+) or negative mode (SM-ESI−). The detector voltage was between 1.3 and 1.7 kV. The samples were dissolved in methanol.

Infrared spectroscopy was performed on a Thermo Scientific Nicolet iS5 spectrometer and data was processed by the OMNIC software. The absorption frequencies were expressed in cm^{-1}. A blank was performed without a sample in the ambient atmosphere. The infrared spectrum of the solid components was performed by intimately grinding the compound and pressing between the diamond and the press.

UV–vis spectroscopy was performed on a Shimadzu UV-1800 spectrometer. The data was recorded and treated using UV-Probe software. The wavelengths were chosen between 200 and 600 nm. The sample was placed in a quartz cuve of 10 mm diameter. The analysis was started right

after the sample preparation and was followed and recorded every minute for 15 min.

Transmission electron microscopy (TEM) images were carried out at the Service de Microscopie Electronique at Fédération de Chimie et Matériaux de Paris-Centre FCMat – Sorbonne Université and recorded with a JEOL TEM 100CXII electron microscope operated at an acceleration voltage of 100 kV. The samples were prepared by the addition of a drop of the stabilized colloid in water on a copper grid coated with a porous carbon film. The images were obtained by the KeenView camera in the ITEM software (1376 × 1032 pixels). The plane and dot resolutions were 0.14 and 0.3 nm, respectively. The size distributions were determined for ≈100 particles, through a manual analysis of enlarged micrographs with ImageJ software using Microsoft Excel to generate histograms of the statistical distribution and a mean diameter.

The EPR analyses were performed at the University of Rennes and have been recorded at room temperature on powders with a BRUKER EMX X-band spectrometer at an excitation frequency of 9.468302 GHz. All liquid samples were lyophilized before the analyses and then put into the glass tube of d = 5 mm.

Synthesis of N-carboxymethyl-N,N-dimethyl-1-hexadecanaminium: Chloroacetic acid (247 mg (2.6 mmol)) were dissolved in absolute ethanol and a saturated solution of sodium hydroxide was slowly added. The reaction mixture was cooled in an ice bath. The white solid was filtered, washed with ethanol, and dried. White solid, m = 190 mg (Yield = 62%). To 504 µL (1.5 mmol, 1equiv.) of *N,N*-dimethylhexadecylamine in H_2O (20 mL), 190 mg (1.63 mmol, 1.1 equiv.) of sodium chloroacetate were added. The reaction mixture was stirred under refluxing for 3 h. Water was removed and the product was dried. m = 480 mg (Yield = 98%), 1H NMR (400 MHz, MeOD, TMS): δ = 0.79 (t, 3H), 1.20 (m, 26H), 1.63 (m, 2H), 3.10 (s, 6H), 3.43 (m, 2H), 3.73 (s, 2H) ppm; ^{13}C NMR (100 MHz, MeOD, TMS): δ = 13.04, 22.33, 26.06–31.67, 50.3, 63.44, 64.21, and 167.45 ppm, IR(C=O)–1627 cm^{-1}.

Manganese Oxide (IV) Suspension Synthesis: 6 mL of an aqueous solution of HEA16Cl (5 equiv.) was added under vigorous stirring to an aqueous solution (4 mL) of the metallic precursor $KMnO_4$ (6 mg, 3.8×10^{-5} mole, 1 equiv.). The solution was heated at 50 °C under continuous stirring for 1 h. The reduction was evidenced by a color change from pink to red and finally to brown. The colloidal suspension was left under continuous stirring overnight before using in an oxidation reaction.

Evaluation in Oxidation of Saturated Hydrocarbons with Mn@HEA16Cl: In a typical reaction, a 100 mL round bottom flask was charged with 5 mL (1.9×10^{-5} mole, 0.0085 equiv.) of colloidal MnO_2 suspension and 2.23 mmol (1 equiv.) of substrate. The aqeous solution was heated at 50 °C under vigorous stirring. After that, 4.46 mmol (2 equiv.) of *tert*-butylhydroperoxide was added under stirring. The reaction mixture was stirred at 50 °C for 7 h 30 min. At the end of the reaction, the organic phase was extracted with 2 × 3 mL of diethylether. The conversion and the selectivity were determined by GC analyses using chlorobenzene as an internal standard. All analyses were performed using TRACE GC ULTRA (Thermo Scientific) with FID detector equipped with a capillary column Thermo Fisher HP5-MS (length 30 m, inside diameter 0.25 mm, film thickness 0.5 µm), with helium as vector gas. The injector and detector temperatures were set at 250 °C. Product identification was performed by comparison of their retention times with commercial pure products.

Supporting Information

Supporting Information is available from the Wiley Online Library or from the author.

Acknowledgements

The authors are grateful to Pr Olivier Cador from UMR-CNRS 6226, Université de Rennes for EPR analyses. The authors are indebted to J.-C. Masteau (Solvay Company, Lyon) for fruitful discussions.

Conflict of Interest

The authors declare no conflict of interest.

Data Availability Statement

The data that support the findings of this study are available in the supplementary material of this article.

Keywords

manganese, nanoworms, oxidation, redox process, water

Received: October 18, 2024
Revised: January 13, 2025
Published online:

[1] K. Philippot, A. Roucoux, *New Trend in the Design of Metal Nanoparticles and Derived Nanomaterials for Catalysis in Nanoparticles in Catalysis: Advances in Synthesis and Applications*, (Eds.: A. Roucoux, K. Philippot), Wiley-VCH Verlag GmbH & Co. KGaA, Weinheim, Germany **2021**, pp. 1–11.
[2] M. Kaushik, A. Moores, *Curr. Opin. Green Sustainable Chem.* **2017**, *7*, 39.
[3] Manganese price in October 2024 was 2.11 $/kg., https://businessanalytiq.com/procurementanalytics/index/manganese-price-index/, (accessed: October 2024).
[4] P. Enghag, *Encyclopedia of the Elements*, Wiley-VCH, Weinheim, Germany **2004**.
[5] K. J. Bell, P. A. Brooksby, M. I. J. Polson, A. J. Downard, *Chem. Commun.* **2014**, *50*, 13687.
[6] Y. Long, J.-F. Hui, P.-P. Wang, S. Hu, B. Xu, G.-L. Xiang, J. Zhuang, X.-Q. Lu, X. Wang, *Chem. Commun.* **2012**, *48*, 5925.
[7] G. Zhang, L. Ren, Z. Yan, L. Kang, Z. Lei, H. Xu, F. Shi, Z.-H. Liu, *Chem. Commun.* **2017**, *53*, 2950.
[8] C. Wei, L. Yu, C. Cui, J. Lin, C. Wei, N. Mathews, F. Huo, T. Sritharan, Z. Xu, *Chem. Commun.* **2014**, *50*, 7885.
[9] D. D. Mal, S. Khilari, D. Pradhan, *Green Chem.* **2018**, *20*, 2279.
[10] Q. Maqbool, C. Singh, P. Jash, A. Paul, A. Srivastava, *Chem.-Eur. J.* **2017**, *23*, 4216.
[11] L. Balan, C. Matei Ghimbeu, L. Vidal, C. Vix-Guterl, *Green Chem.* **2013**, *15*, 2191.
[12] C. Yao, J. Wang, A. Zheng, L. Wu, X. Zhang, X. Liu, *Sens. Actuators, B* **2017**, *252*, 30.
[13] J. Xiao, P. Liu, Y. Liang, H. B. Li, G. W. Yang, *J. Appl. Phys.* **2013**, *114*, 073513.
[14] J. Wu, Q. Wang, A. Umar, S. Sun, L. Huang, J. Wang, Y. Gao, *New J. Chem.* **2014**, *38*, 4420.
[15] S. Ghosh, B. Gupta, K. Ganesan, A. Das, M. Kamruddin, S. Dash, A. K. Tyagi, *Mater. Today Proc.* **2016**, *3*, 1686.
[16] C. M. Julien, A. Mauger, *Nanomaterials* **2017**, *7*, 396.
[17] W. He, W. Yang, C. Wang, X. Deng, B. Liu, X. Xu, *Phys. Chem. Chem. Phys.* **2016**, *18*, 15235.
[18] W. Wei, X. Cui, W. Chen, D. G. Ivey, *Chem. Soc. Rev.* **2011**, *40*, 1697.
[19] S. K. Ramchandra, C. Min-Seung, Y. Kwi-Sub, K. Tae-Sin, P. Chan-Jin, *Nanotechnology* **2011**, *22*, 395402.
[20] Y. Meng, W. Song, H. Huang, Z. Ren, S.-Y. Chen, S. L. Suib, *J. Am. Chem. Soc.* **2014**, *136*, 11452.
[21] E. Saputra, S. Muhammad, H. Sun, H. M. Ang, M. O. Tadé, S. Wang, *Environ. Sci. Technol.* **2013**, *47*, 5882.
[22] Y. Yang, J. Huang, S. Wang, S. Deng, B. Wang, G. Yu, *Appl. Catal. B* **2013**, *142–143*, 568.

[23] H.-Y. Sun, Q. Hua, F.-F. Guo, Z.-Y. Wang, W.-X. Huang, *Adv. Synth. Catal.* **2012**, *354*, 569.
[24] Y. Yamaguchi, R. Aono, E. Hayashi, K. Kamata, M. Hara, *ACS Appl. Mater. Interfaces* **2020**, *12*, 36004.
[25] K. Kamata, N. Kinoshita, M. Koutani, R. Aono, E. Hayashi, M. Hara, *Catal. Sci. Technol.* **2022**, *12*, 6219.
[26] A. Shaabani, Z. Hezarkhani, E. Badali, *Polyhedron* **2016**, *107*, 176.
[27] A. S. Burange, S. R. Kale, R. V. Jayaram, *Tetrahedron Lett.* **2012**, *53*, 2989.
[28] Z. Hu, Y. Zhao, J. Liu, J. Wang, B. Zhang, X. Xiang, *J. Colloid Interface Sci.* **2016**, *483*, 26.
[29] E. Roduner, W. Kaim, S. Biprajit, V. B. Urlacher, J. Pleiss, R. Gläser, W.-D. Einicke, G. A. Sprenger, U. Beifuss, E. Klemm, C. Liebner, H. Hieronymus, S.-F. Hsu, B. Plietker, S. Laschat, *ChemCatChem* **2013**, *5*, 82.
[30] A. V. Kharlamov, O. I. Artyushin, N. A. Bondarenko, *Russ. Chem. Bull.* **2014**, *63*, 2445.
[31] S. A. Alzahrani, S. A. Al-Thabaiti, W. S. Al-Arjan, M. A. Malik, Z. Khan, *J. Mol. Struct.* **2017**, *1137*, 495.
[32] L. Sanchez-Botero, A. P. Herrera, J. P. Hinestroza, *Nanomaterials* **2017**, *7*, 117.
[33] S. E. Lohse, C. J. Murphy, *Chem. Mater.* **2013**, *25*, 1250.
[34] S. Mallakpour, F. Motirasoul, *RSC Adv.* **2016**, *6*, 62602.
[35] Z. Khan, S. A. Al-Thabaiti, A. Yousif Obaid, Z. A. Khan, *Colloids Surf., B* **2010**, *81*, 381.
[36] J. Cui, L. Xi, B. Zhang, X. Mao, *Chem. Eng. J.* **2017**, *313*, 815.
[37] K. Selvakumar, S. M. Senthil Kumar, R. Thangamuthu, G. Kruthika, P. Murugan, *Int. J. Hydrogen Energy* **2014**, *39*, 21024.
[38] A. Denicourt-Nowicki, A. Lebedeva, C. Bellini, A. Roucoux, *ChemCatChem* **2016**, *8*, 357.
[39] A. Lebedeva, B. L. Albuquerque, J. D. Domingos, J.-F. Lamonier, J.-M. Giraudon, P. Lecante, A. Denicourt-Nowicki, A. Roucoux, *Inorg. Chem.* **2019**, *58*, 4141.
[40] K. Godula, D. Sames, *Science* **2006**, *312*, 67.
[41] S. Alini, P. Babini, *Handbook of Advanced Methods and Processes in Oxidation Catalysis*, Imperial College Press, London, UK, **2014**, pp. 320–333.
[42] F. Näf, R. Decorzant, *Helv. Chim. Acta* **1978**, *61*, 2524.
[43] D. Prat, A. Wells, J. Hayler, H. Sneddon, C. R. McElroy, S. Abou-Shehada, P. J. Dunn, *Green Chem.* **2016**, *18*, 288.
[44] E. C. McLaughlin, H. Choi, K. Wang, G. Chiou, M. P. Doyle, *J. Org. Chem.* **2009**, *74*, 730.
[45] A. Corma, S. Iborra, A. Velty, *Chem. Rev.* **2007**, *107*, 2411.
[46] M. Bohnet, *Ullmann's Encyclopedia of Industrial Chemistry*, 6th ed., Wiley-VCH, Weinheim, Germany **2003**.

